Fusion of $^{16}O + ^{165}Ho$ at deep sub-barrier energies

Saikat Bhattacharjee,[1,3] A. Mukherjee,[1,3,*] Ashish Gupta,[1,3] Rajkumar Santra,[1,3] D. Chattopadhyay,[1,†] N. Deshmukh,[1,‡] Sangeeta Dhuri,[2,3] Shilpi Gupta,[2,3] V. V. Parkar,[2,3] S. K. Pandit,[2] K. Ramachandran,[2] K. Mahata,[2,3] A. Shrivastava,[2,3] Rebecca Pachuau,[4,§] and S. Rathi[5]

[1]*Saha Institute of Nuclear Physics, 1/AF, Bidhan Nagar, Kolkata 700064, India*
[2]*Nuclear Physics Division, Bhabha Atomic Research Centre, Mumbai 400085, India*
[3]*Homi Bhabha National Institute, Anushaktinagar, Mumbai 400094, India*
[4]*Tata Institute of Fundamental Research, Mumbai 400005, India*
[5]*Vivekanand Education Society's College of Arts, Science and Commerce, Mumbai 400071, India*

(Received 8 April 2021; revised 6 October 2021; accepted 26 October 2021; published 17 November 2021)

Fusion cross sections have been measured for the asymmetric system $^{16}O + ^{165}Ho$ at energies near and deep below the Coulomb barrier with an aim to investigate the occurrence of fusion hindrance for the system. Cross sections down to ≈700 nb have been measured using the off-beam γ-ray technique. The fusion cross sections have been compared with the coupled channel calculations. The energy onset of fusion hindrance appears to occur at $E_{\mathrm{c.m.}} = 57 \pm 0.85$ MeV, where a deviation in the slope of the experimental logarithmic derivative compared to that of coupled channel calculations has been observed. This is in agreement with the value obtained from the touching point configuration of the adiabatic model.

DOI: 10.1103/PhysRevC.104.054607

I. INTRODUCTION

Extensive studies on fusion reactions at sub-barrier energies in different mass regions have unraveled the fundamentals of quantum mechanical tunneling and distribution of potential barriers between two interacting nuclei. Fusion in the vicinity of Coulomb barrier is a probe to discern the indispensable role of different intrinsic features of the interacting nuclei on the reaction process. Enhancement of fusion cross sections observed in heavy-ion collisions at sub-barrier energies has been well explained by the coupled channels model [1,2].

On extending the measurements from sub-barrier down to deep sub-barrier energies, for a wide range of reactions [3–19], a steep fall-off of fusion excitation function has been observed compared to the standard coupled channels calculations, although fusion cross sections are still enhanced with respect to single-barrier penetration model calculations. This phenomenon of change of slope in the fusion excitation function at deep sub-barrier energies is termed "fusion hindrance." Observation of fusion hindrance at deep sub-barrier energies, especially in light systems like $^{12}C + ^{12}C$; $^{16}O + ^{16}O$ [4] have astrophysical implications, as some of the light systems transpire in the late evolutionary stages of massive stars.

Fusion hindrance was initially observed in the symmetric medium-heavy system $^{60}Ni + ^{89}Y$ [3], having negative Q value. Subsequently, studies of several symmetric and nearly symmetric [5–13] and asymmetric [14,15] systems over a wide range of mass and fusion Q values have also been similarly observation. Direct evidence of hindrance for fusion of weakly bound light projectiles $^{6,7}Li$ with ^{198}Pt target has not been observed yet, at deep sub-barrier energies [16,17]. Recently, dominance of breakup channel at deep sub-barrier energy has been observed in the reaction of the proton halo nucleus ^{8}B with ^{208}Pb [20]. It has been reported that at a laboratory energy of 30 MeV (20 MeV below the barrier) the breakup channel almost exhausts the total reaction cross section, thereby indicating fusion to be hindered for this system at deep sub-barrier. Moreover, in fusion with relatively heavier and strongly bound projectile ^{12}C on the target ^{198}Pt [16], hindrance has been directly observed. For lighter $^{11}B + ^{197}Au$ system [18], the degree of hindrance appears to be weaker in nature. In the background of this scenario, it appears that investigation of the phenomenon of deep sub-barrier fusion hindrance for numerous other asymmetric systems over a wide range of projectiles and targets may shed some light into the deeep sub-barrier fusion dynamics.

Several models with different physical foundations have been proposed to describe this phenomenon. Among them, the model developed by Mişicu and Esbensen [21,22] is based on sudden approximation. A soft repulsive core was incorporated with the density folded M3Y potential in this model, to consider the nuclear incompressibility in the overlapping region of the two interacting nuclei. The adiabatic model proposed by Ichikawa *et al.* [23,24] introduces an additional damping factor on the nuclear coupling potential. The damping factor

*anjali.mukherjee@saha.ac.in
†Present adddress: Tata Institute of Fundamental Research, Mumbai 400005, India.
‡Present address: School of Sciences, Auro University, Surat, Gujarat 394510, India.
§Present address: Department of Physics, Banaras Hindu University, Varanasi 221005, India.

is a function of the internuclear distance, which takes into consideration of the smooth change from sudden to adiabatic transition while the two nuclei are going through fusion deep below the barrier. More recently, Simenel *et al.* have studied the effect of Pauli repulsion on heavy-ion fusion by implementing the density-constrained frozen Hartree-Fock method [25]. Despite having different physical origins, these models have been quite successful in reproducing the experimental results for different systems at deep sub-barrier energies [4]. In the light of the problem of fusion hindrance, we have recently measured fusion cross sections for ^{16}O + ^{165}Ho system at energies near and deep below the Coulomb barrier. Owing to the large deformation of nuclei in the rare-earth-metal region, systems involving such nuclei usually exhibit strong coupling effects between relative motion and internal degrees of freedom in the sub-barrier fusion mechanism. The target nucleus ^{165}Ho has a large deformation parameter [26], whereas the projectile ^{16}O is a tightly bound spherical nucleus and therefore subdues the projectile effect of different coupling schemes on the fusion mechanism. It has been perceived that stiff systems, where coupling effects are small, typically show fusion hindrance more readily than soft systems [4]. The dominance of the influence of different direct reaction channels, like inelastic scattering, transfer, and breakup, in reactions involving soft nuclei are believed to be responsible for the occurrence of fusion hindrance at much lower energies than stiff systems [4]. The system ^{16}O + ^{165}Ho lies between stiff and soft systems having a negative Q value ($Q = -23.1$ MeV) for fusion. It would be interesting to study fusion mechanism in the system of tightly bound projectile ^{16}O on the deformed nucleus ^{165}Ho, especially at deep sub-barrier energies.

The complete fusion (CF) cross sections of ^{16}O + ^{165}Ho at above-barrier energies have been reported in the literature [27]. The present study overlaps some of the energies of the reported measurement. The measurement has been extended below barrier to deep sub-barrier energy region. An off-beam γ-ray detection technique has been implemented to measure the cross sections of the β-active evaporation residues. Section II recounts the detailed experimental method that have been implemented to perform the experiment. The procedure of data analysis have been explained in Sec. III. The details of theoretical coupled channel calculations and comparison with experimental results have been described in Sec. IV. Section V consists of a discussion followed by a summary of the present work in Sec. VI.

II. EXPERIMENTAL DETAILS

The experiment was performed at the 14UD BARC-TIFR Pelletron-LINAC facility, Mumbai. Self-supporting, rolled, natural foils of ^{165}Ho, having thickness in the range ≈1.02–1.9 mg/cm^2 were irradiated by beams of ^{16}O, in the energy range $E_{\rm lab} = 62$–85 MeV. Each target foil of ^{165}Ho was followed by an Al catcher foil, sufficiently thick to stop the heavy evaporation residues (ERs) produced in the reaction. The thickness of each target and catcher foil was measured by the α-transmission method. For each irradiation, a fresh target-catcher foil assembly was used. Typical beam current during the irradiations was ≈2–10 pnA. To correct for

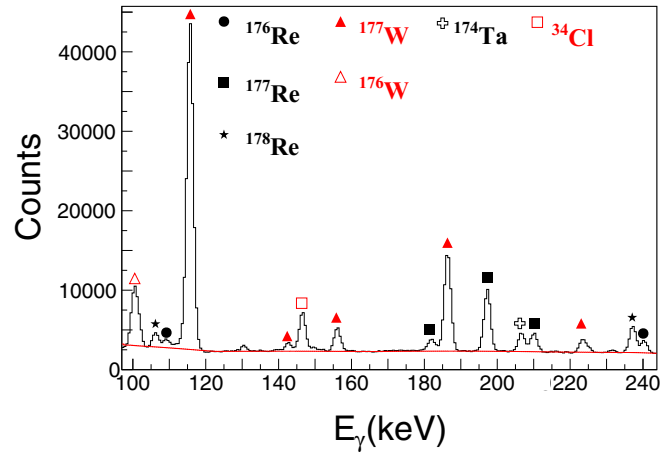

FIG. 1. γ-ray spectrum of the evaporation residues arising from the complete fusion (CF) of ^{16}O + ^{165}Ho system at 84-MeV beam energy. The red line is the background estimated by ROOT data analysis package [29].

beam fluctuations during the irradiation, the beam current was recorded at regular intervals of 1 min using a Computer-Aided Measurement And Control (CAMAC) scaler. The energies of the incident beam were corrected for the loss of energy in the target material by employing Stopping and Range of Ions in Matter (SRIM) [28], at half-thickness of the target. As all the ERs were β active and yielded delayed γ rays, the activation technique was employed to determine the fusion cross sections for the system. After each irradiation, the target-catcher foil assembly was removed from the chamber and placed in front of an efficiency-calibrated HPGe detector, which detected the delayed γ rays emitted by the ERs.

The target-catcher foil assembly was placed either at a distance of 10 cm from the face of the detector or on the face of the detector, depending on the activity of the irradiated sample. The energy calibration and absolute efficiency measurement of the detector were carried out using the standard radioactive sources, ^{152}Eu, ^{133}Ba, and ^{60}Co, mounted in the same geometry as the target. The measurement was done in a low background setup with Pb-Cu graded shielding to reduce the background γ rays. Data were recorded using a digital data acquisition system employing a CAEN N6724 digitizer and the data were analyzed using the ROOT data analysis framework [29]. A typical off-beam γ-ray spectrum, after the irradiation at $E_{\rm lab} = 84$ MeV, is shown in Fig. 1. The complete fusion ERs $^{176-178}$Re occurring from the decay of the compound nucleus ^{181}Re were uniquely identified from the characteristic γ rays emitted by their daughter nuclei and by following the half-lives (see Table I). Half-lives of the ERs were measured from the time-sliced yields of the characteristic γ rays and compared with the previously measured values [30], to ensure the absence of any contribution from sources other than the complete fusion residues. The half-life plot for ^{178}Re at $E_{\rm lab} = 70$ MeV has been shown in Fig. 2.

III. ANALYSIS AND RESULTS

If N_γ represents the number of counts under a particular γ-ray peak, corresponding to a given ER in the spectrum, then

TABLE I. Spectroscopic properties of the evaporation residues, resulting via CF process that have been used to calculate the CF cross sections for the $^{16}O + ^{165}Ho$ system.

Residue	$T_{1/2}$ (min)	J^{π}	E_{γ} (keV)	I^{γ} (%)
$^{178}Re(3n)$	13.2	3^+	237.0	44.5
			106.0	23.4
$^{177}Re(4n)$	14.0	$5/2^-$	196.9	8.4
			209.8	2.8
$^{176}Re(5n)$	5.3	3^+	240.3	54.0
			109.1	25.0
$^{174}Ta(\alpha 3n)$	68.4	3^+	206.5	60.0

from the principle of radioactive decay the corresponding ER cross section (σ_{ER}) is given as [31]

$$\sigma_{ER} = \frac{N_{\gamma}\lambda e^{\lambda t_w}}{N_B N_T \epsilon_{\gamma} F_{\gamma}(1 - e^{-\lambda t_c})(1 - e^{-\lambda t_{irr}})}, \quad (1)$$

where N_B is the number of incident nuclei, N_T is the number of target nuclei per unit area, λ is the decay constant of the ER, t_{irr} is the irradiation time, t_w is the time elapsed between the end of irradiation and the beginning of counting, t_c is the counting time, ϵ_{γ} is the efficiency of the detector for a given γ-ray energy, and F_{γ} is the absolute intensity of a γ-ray decay.

The γ-ray peak corresponding to ^{34}Cl, seen in the spectrum (Fig. 1), arises from the reaction of ^{16}O with the Al catcher foil. Different *pxn* and αxn channels, corresponding to isotopes of W and Ta respectively, populated in the reaction of $^{16}O + ^{165}Ho$ are marked in the spectrum. The *pxn* channel can be populated as an ER of compound nucleus and also from the decay product of Re (e.g., $^{177}Re \xrightarrow{\epsilon} {}^{177}W$). The procedure to calculate the true weight of *pxn* ERs from the cumulative cross sections have been discussed by Cavinato *et al.* [32].

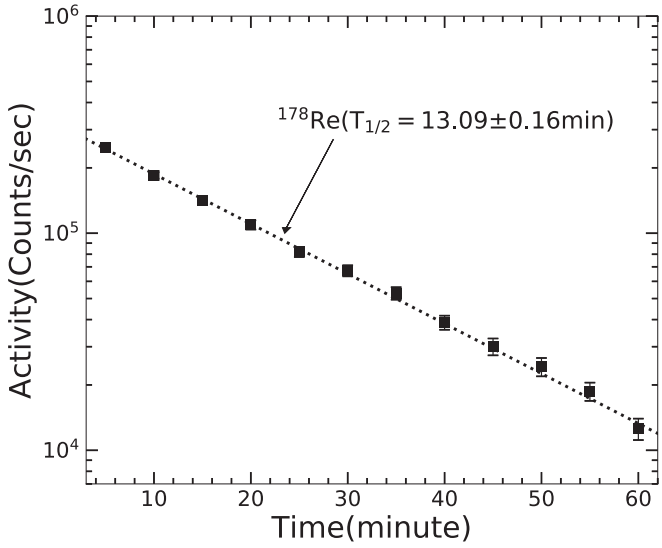

FIG. 2. Activity of the ^{178}Re evaporation residue as a function of progressing time at $E_{lab} = 70$ MeV. The dotted line corresponds to the activity obtained by fitting the data. The half-life from the fit is mentioned in the graph, which is consistent with the known value.

TABLE II. Neutron and α potential parameters used for PACE4 calculations.

Neutron				Alpha			
V_0 (MeV)	r_V, a_V (fm)	W_0 (MeV)	r_W, a_W (fm)	V_0 (MeV)	r_V, a_V (fm)	W_0 (MeV)	r_W, a_W (fm)
30.0	1.219, 0.688	8.0	1.282, 0.512	154.18	1.245, 0.77	20.08	1.57, 0.582

In the energy region of the present measurement, it has been found that majority of the γ-ray peaks corresponding to *pxn* channels are due to the decay of Re nuclei. The contribution of *pxn* ERs, i.e., the direct decay product of compound nucleus, falls within the error limit of respective cross sections at different energies and thus have not been estimated rigorously. The αxn channels are populated either by incomplete fusion (ICF) or via the decay of compound nucleus (CF). To estimate the contribution of αxn channels arising from the CF residues, a statistical model calculation has been performed using the PACE4 code [33].

To obtain a relatively better agreement between theoretical and experimental cross sections, the neutron and α potentials in the code have been modified according to Refs. [34,35], respectively.

Although there is an energy dependence in the neutron potential form, the change in potential parameters are small with change in energy. It has been observed that the PACE4 calculation is not affected significantly by the small changes in potential parameters. Hence, average values of potential parameters have been used throughout the calculation (see Table II). Fission barrier was fixed at 21.89 MeV following Ref. [27]. It has been observed that varying the level density parameter k within a range of 8–10 does not significantly affect the statistical model calculation [27]. Hence, the parameter k was fixed at 9 throughout the calculations. The other parameters in the code were set to the default values. Calculated cross section for each partial wave by coupled channel calculation (detailed discussion in next section) has been fed as input to the PACE4 calculations. The production of ^{174}Ta via ICF is energetically possible at higher energies (80–85 MeV) but at lower energies, it becomes unlikely that ^{174}Ta will be populated as an ICF product. It has also been observed that within the energy range of the measurement, the experimental cross sections of $\alpha 3n$ channel (^{174}Ta) reasonably agree with the statistical model, which exclusively deals with CF process. The experimentally measured cross sections of other αxn channels are distinctly underestimated by the statistical model calculations. A similar trend has also been observed in Ref. [27]. As the PACE4 code has been able to reproduce the cross sections of *xn* and $\alpha 3n$ channels relatively well, it can be inferred that all the other αxn channels, or at least an exceedingly significant part of them, have been populated via incomplete fusion (ICF). Figure 3 shows a comparison of the statistical model calculations with the measured ER channel cross sections. For this system, ICF processes are important reaction channels at energies above barrier. It has been found that the ICF contribution for this system switches

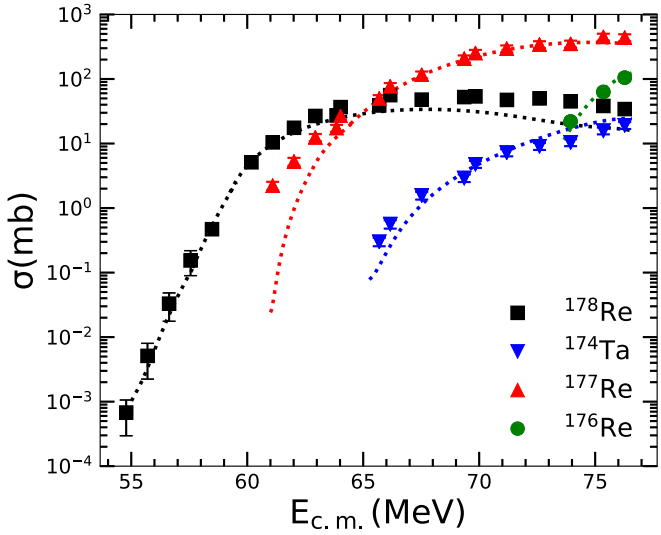

FIG. 3. The cross-sections of different evaporation residues of compound nucleus for $^{16}O + ^{165}Ho$ system. The dotted lines are the statistical model calculation (PACE4) results.

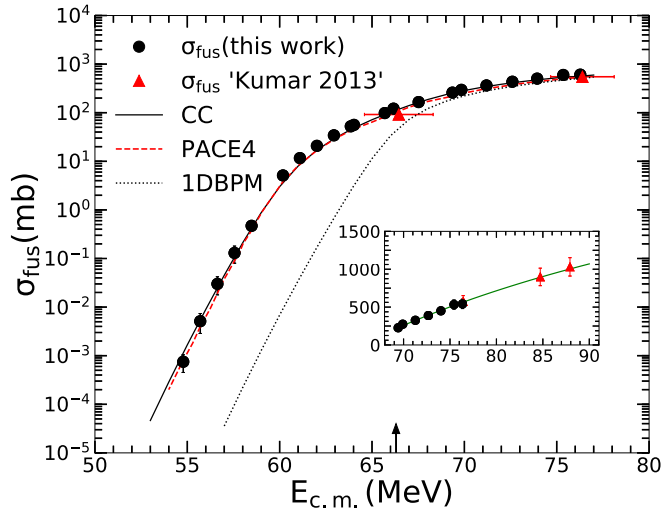

FIG. 4. Complete fusion excitation function measured in this experiment and the previous measurement (Kumar 2013: [27]) has been compared with coupled channel (CC) calculations using Woods-Saxon potential form. The solid lines are the results obtained from the CC calculations. The arrow corresponds to the Coulomb barrier for this system. The dashed curve shows the fusion cross sections obtained from the PACE4 calculations. (Inset) Fusion cross section at above barrier energies are fitted with Wong formula to obtain the optical model potential parameters of the system. The solid line shows the fitted results. The x-axis corresponds to Ec.m. (MeV) and the y-axis corresponds to fusion cross-section (mb).

off at some energy value between $E_{\text{c.m.}} = 76.4$–66.5 MeV [27], thereby showing that fusion cross sections below the barrier have no ICF contribution. Hence, it can be concluded that the ICF channels have no influence at below-barrier and deep sub-barrier energies for this system.

The ERs that have been considered in determining the CF cross sections are ^{176,177,178}Re and ^{174}Ta. Due to their low cross sections (<5% aggregate contribution), the *pxn* channels ^{176,177,178}W have not been added into the CF cross sections, bearing in mind the difficulty of getting the exact cross sections for this channels and large errors involved. It should be noted that the statistical model calculations have solely been implemented to compare the experimental cross-sections for each CF channel and to eliminate the ICF channels. No other PACE4 input has been taken in estimating the experimental cross sections.

The total fusion cross sections have been determined by adding the measured cross sections of *xn* and $\alpha 3n$ channels and are shown in Fig. 4. Fusion cross section down to 678 nb has been measured in this work. Statistical errors, as well as errors ensuing from the measurement of beam current, target thickness, and detector efficiency, have been taken into account. The dashed curve in the figure shows the fusion cross sections as predicted by the PACE4 calculations. The astrophysical S factor, often used in nuclear astrophysics to study the low-energy behavior of nuclear reactions, is defined as

$$S(E) = E\sigma(E)\exp(2\pi\eta), \tag{2}$$

where E is the center-of-mass energy, σ is the fusion cross section, and $\eta = Z_1 Z_2 e^2/\hbar v$ is the Sommerfield parameter with v being the relative velocity in center-of-mass frame. The experimental S factor curve corresponding to the measured fusion cross sections for the present system has been plotted in Fig. 5(a). Appearance of a maximum in the S-factor curve has been presented in previous studies at an energy where the hindrance in fusion cross section sets in. In the present study, although no clear maximum could be seen in the S-factor curve within the measured energy range, an indication of a change of slope at the lowest energy could be observed. An

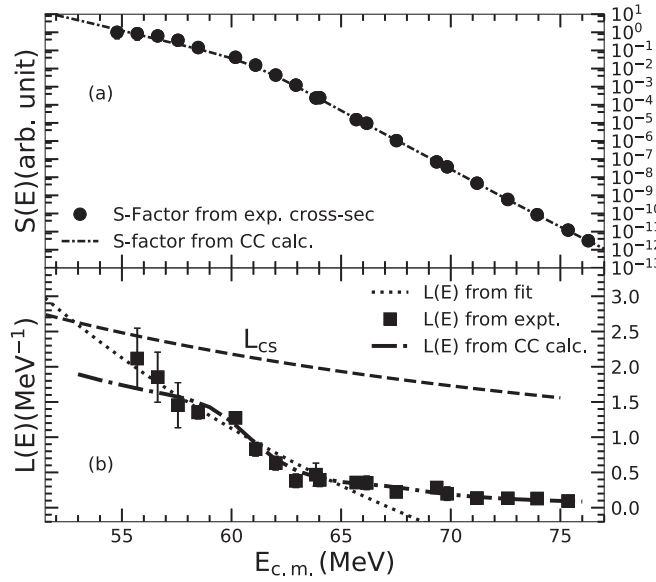

FIG. 5. (a) Astrophysical S factor for $^{16}O + ^{165}Ho$ system compared with S factor obtained from CC calculation. (b) Logarithmic derivative $L(E)$ of the experimental fusion excitation function compared with CC calculations (dash-dotted lines).

alternative representation, the logarithmic slope of the fusion excitation function is defined as [3]

$$L(E) = d[\ln(E\sigma)]/dE = \frac{1}{E\sigma}\frac{d(E\sigma)}{dE}. \quad (3)$$

The values of $L(E)$ extracted from the measured fusion cross sections for $^{16}O + ^{165}Ho$ are plotted in Fig. 5(b). These representations are independent of any theoretical model and are alternative approaches to manifest any deviation in the slope of excitation function. From Eqs. (2) and (3), one gets the relation

$$\frac{dS}{dE} = S(E)\Big[L(E) - \frac{\pi\eta}{E}\Big]. \quad (4)$$

The derivative $\frac{dS}{dE}$ becomes zero when the S factor becomes maximum, and from Eq. (3) one finds that this corresponds to the logarithmic derivative for constant S factor, $L_{cs}(E)$, given by

$$L_{cs}(E) = \frac{\pi\eta}{E} \quad (5)$$

The curve $L_{cs}(E)$ for the present system is shown in Fig. 5(b) by the dashed line. The experimental values of $L(E)$ have been fitted with a function $A + B/E^{\frac{3}{2}}$ [36,37], and is shown in Fig. 5(b) by the dotted line. The crossover point of the curves $L_{cs}(E)$ and fitted $L(E)$ corresponds to the maximum of the S-factor curve [4]. The change in slope of $L(E)$ occurs at around 57 ± 0.85 MeV, which is related to the threshold energy (E_s) for the occurrence of fusion hindrance [38]. It can be seen from Fig. 5(b) that an extrapolation of the fitted $L(E)$ curve intersects the curve $L_{cs}(E)$ at the energy 52.78 ± 0.78 MeV, which corresponds to the energy onset of S-factor maximum. The value of E_s calculated from the empirical equation [39] is 53.17 MeV. The estimation of E_s obtained from the touching point configuration in adiabatic picture [23,24] is 56.1 MeV. The present measurement has been performed down to $E =$ 54.78 MeV. This shows that the E_s value $^{16}O + ^{165}Ho$ system is consistent with the adiabatic model, within the limits of uncertainty, if we consider the energy at which the change of slope in $L(E)$ occurs.

IV. COMPARISON WITH COUPLED CHANNELS CALCULATIONS

The data obtained in the present work have been analyzed in the framework of coupled channels (CC) calculations, using the code CCFULL [40]. These calculations require an initial set of potential parameters. They were obtained by fitting the fusion cross sections well above the barrier using Wong's formula [41], as the fusion cross sections in this energy regime are expected to be fairly insensitive to the form or magnitude of the couplings. The nuclear potential was taken to be of Woods-Saxon form,

$$V_n(r) = \frac{-V_0}{1 + \exp\big[\big(r - r_0A_P^{1/3} - r_0A_T^{1/3}\big)/a\big]}, \quad (6)$$

where V_0 is the depth, r_0 is the radius parameter, and a is the diffuseness of the nuclear potential. The potential parameters were obtained by fixing a to be 0.63 fm, and varying r_0 and V_0 to obtain a good fit to the high energy part of the cross sections. The parameters thus obtained are $V_0 = 102$ MeV, $r_0 = 1.15$ fm, and $a_0 = 0.63$ fm. The inset in Fig. 4 shows the resulting fit. The potential parameters for the same system have also been compared with Ref. [42]; both results are found to be identical.

The CCFULL calculations in the no-coupling limit are shown by the dotted curve in Fig. 4, and are seen to underpredict the data, suggesting strong effects of deformation in the target nucleus. The CCFULL code estimates the effects of deformation by linear as well as nonlinear coupling to the pure rotational bands of the deformed nucleus. The target nucleus ^{165}Ho is deformed with a valence proton. The rotational states of ^{165}Ho may be considered to be built up by the coupling of the unpaired valence proton particle (or proton hole) with the $0^+, 2^+, 4^+$,... rotational states of the neighboring even-even nucleus ^{164}Dy (or ^{166}Er). To remain within the model space of CCFULL, the excitation energies and deformation parameters for the target nuclues ^{165}Ho were taken to be the averages of those of the neighboring even-even nuclei ^{164}Dy and ^{166}Er [43,44]. The resulting ground state rotational band up to 12^+ state ($\beta_2 = 0.32$, $\beta_4 = 0.02$) was included in the calculations. The results of these calculations are shown by the solid curve in the figure. They are seen to be in fairly good agreement with the data, except the lowest energy data which appears to be slightly below the calculated value.

The solid curve in Fig. 5(a) shows the calculated astrophysical S-factor values extracted from the CC cross sections and are found to agree well with the experimental value, except the lowest energy point. Although no clear maximum in the experimental S-factor plot or deviation from the the CC calculations could be observed in the measured energy range, an indication of a small deviation could be seen at the lowest energy measured. The dot-dashed curve in Fig. 5(b) shows the calculated $L(E)$ values extracted from the CC cross sections are also seen to agree well with the experimental values, although the trend of the two extreme low-energy points show an indication of possible deviation at still lower energies.

V. DISCUSSION

For a systematic study of the energy onset of fusion hindrance, the value of E_s predicted for the system $^{16}O + ^{165}Ho$ in the present work has been compared in Fig. 6 with the E_s values of other heavy systems as a function of the system parameter $\zeta = Z_pZ_t\sqrt{\frac{A_pA_t}{A_p+A_t}}$. The parameters A_p, Z_p, A_t, Z_t are the mass number and atomic number of projectile and target. In this comparison, we have considered only the systems in the ζ range $\approx$1500–3000. For each of the systems, E_s has been obtained from the change in slope of experimental logarithmic derivate with respect to CC calculations [16,38]. The parameter ζ contains information of the mass and Coulomb barrier of the target-projectile system. The dashed line in the figure corresponds to the empirical form of E_s [39]. The value of E_s obtained from the slope change of $L(E)$ in the present work, lies above the dashed line obtained from the empirical form $E_s^{\rm emp} = [0.495\zeta/(2.33 + 580/\zeta)]^{2/3}$, in agreement with the other systems in this range of ζ. The systems $^{48}Ca + ^{48}Ca$ [10]

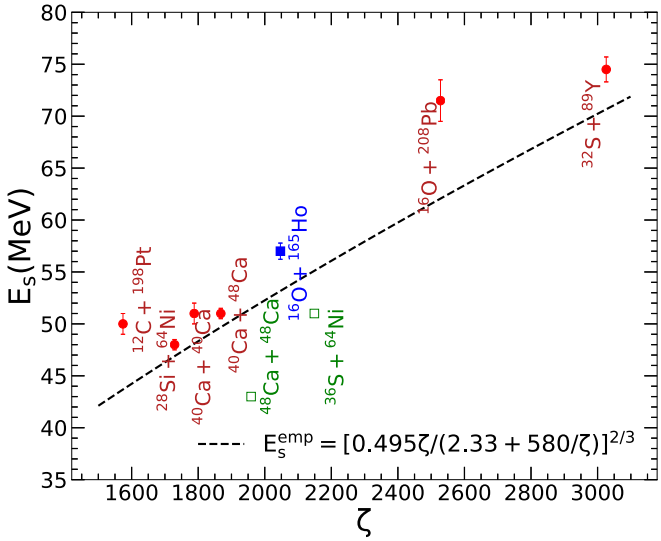

FIG. 6. Systematic representation of E_s as a function of system parameter ζ. The solid circles are the values of E_s, obtained from the slope change in experimental log derivative with respect to CC calculations for the systems in Refs. [9,14,16,45–47]. The solid square represents the E_s value obtained in this work. The hollow squares correspond to Refs. [10,48] where the value of E_s cannot be obtained either by extrapolation or direct measurements and an upper bound has been mentioned in Ref. [4].

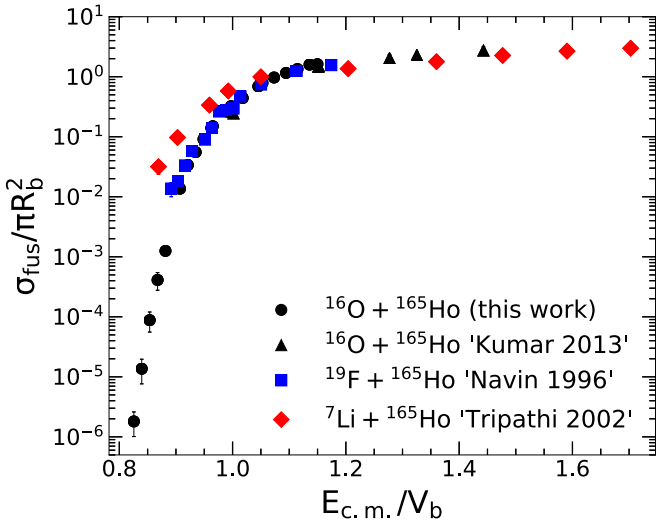

FIG. 7. Comparison of normalized fusion excitation function between $^{16}O + ^{165}Ho$ (in this work and Kumar 2013 [27]), $^{19}F + ^{165}Ho$ (Navin 1996 [49]), and $^{7}Li + ^{165}Ho$ (Tripathi 2002 [50]) systems.

and $^{36}S + ^{64}Ni$ [48] ($\zeta = 1959$ and 2149 respectively) also fall within the ζ range in Fig. 6, but none of the systems has exhibited any signature of fusion hindrance upto the measured energy range. An upper bound of the E_s has been mentioned in Ref. [4] for these two systems.

It should be noted that the value of E_s can also be estimated from the crossover point of experimental $L(E)$ and $L_{CS}(E)$. This prescription has been used in Ref. [4] to tabluate the E_s values of different systems, spanning a wide range of ζ. The crossover point represents the energy onset of S-factor maximum, below which a change in slope of experimental curve can clearly be observed for systems that exhibit fusion hindrance. This approach is independent of any model calculations and particularly useful for low-mass systems of astrophysical importance, where direct measurement of fusion cross section is difficult to conceive and extrapolation is required to estimate the E_s values. It is obvious that the slope change method which has been implemented in this work returns the value of E_s a few MeV above than that obtained from crossover point. It can be inferred that the change in slope of experimental $L(E)$ provides the energy onset of fusion hindrance; while at the crossover point, the fusion hindrance can distinctly be observed.

A systematic comparison of fusion excitation functions have been carried out for systems involving the target nucleus ^{165}Ho and different projectiles and is shown in Fig. 7. The systems involving ^{165}Ho target nucleus, for which sub-barrier fusion cross sections have been reported in literature are $^{19}F + ^{165}Ho$ [49] and $^{7}Li + ^{165}Ho$ [50]. The projectile ^{16}O in the present system is a stiff nucleus, while ^{19}F is relatively heavier and less bound than ^{16}O, and ^{7}Li is a well-known weakly bound stable nucleus. For comparison of different projectile-target systems, the fusion excitation functions have been plotted in a reduced scale. Barrier radii $R_b = r_0(A_p^{\frac{1}{3}} + A_t^{\frac{1}{3}})$ and Coulomb barrier V_b for each system was obtained by performing 1DBPM model calculation, using the Akyüz-Winther parametrization of Woods-Saxon potential [51]. The values of R_b and V_b is provided in Table III.

Figure 7 shows that the reduced fusion excitation functions for the three systems overlap reasonably well with each other at above barrier energies, but there are no reported fusion cross sections at deep-sub-barrier energies for the systems $^{19}F + ^{165}Ho$ and $^{7}Li + ^{165}Ho$. At sub-barrier energies, the fusion cross sections for $^{19}F + ^{165}Ho$ and $^{16}O + ^{165}Ho$ agree fairly well with each other, while the fusion cross sections for $^{7}Li + ^{165}Ho$ are enhanced in the reduced scale. It would be interesting to see how the deep sub-barrier fusion cross sections for the two systems compare with the present $^{16}O + ^{165}Ho$ system.

VI. SUMMARY

The fusion cross sections for $^{16}O + ^{165}Ho$ have been measured down to 678 nb, from above-barrier to deep sub-barrier energies. The present measurement agrees with the earlier

TABLE III. V_b and R_b of the systems that have been used in the reduced plot (Fig. 7).

System	V_b (MeV)	R_b (fm)
$^{16}O + ^{165}Ho$	66.34	10.93
$^{19}F + ^{165}Ho$	72.24	11.26
$^{7}Li + ^{165}Ho$	25.0	10.76

reported data [27], in the overlapping above-barrier energy region. Statistical model calculation of different evaporation residues occurring from CF yielded similar results with experimental data. The experimental CF cross sections have been well reproduced by the coupled-channels calculations.

The logarithmic slope and the astrophysical S-factor have been extracted from the measured and CC calculated fusion excitation functions. The change in slope of $L(E)$ compared to the $L(E)$ obtained from CC calculations suggests the onset of fusion hindrance at 57 ± 0.85 MeV, in accordance with the prediction from adiabatic model.

ACKNOWLEDGMENTS

We sincerely thank the staff of BARC-TIFR Pelletron facility for an uninterrupted supply of beam. We would like to extend our gratitude to Dr. Sanjoy Pal of TIFR, Mumbai, for helping with the digital data acquisition.

[1] A. B. Balantekin and N. Takigawa, Rev. Mod. Phys. **70**, 77 (1998), and references therein.
[2] M. Dasgupta, D. J. Hinde, N. Rowley, and A. M. Stefanini, Annu. Rev. Nucl. Part. Sci. **48**, 401 (1998), and references therein.
[3] C. L. Jiang, H. Esbensen, K. E. Rehm, B. B. Back, R. V. F. Janssens, J. A. Caggiano, P. Collon, J. Greene, A. M. Heinz, D. J. Henderson, I. Nishinaka, T. O. Pennington, and D. Seweryniak, Phys. Rev. Lett. **89**, 052701 (2002).
[4] B. B. Back, H. Esbensen, C. L. Jiang, and K. E. Rehm, Rev. Mod. Phys. **86**, 317 (2014), and references therein.
[5] C. L. Jiang, K. E. Rehm, R. V. F. Janssens, H. Esbensen, I. Ahmad, B. B. Back, P. Collon, C. N. Davids, J. P. Greene, D. J. Henderson, G. Mukherjee, R. C. Pardo, M. Paul, T. O. Pennington, D. Seweryniak, S. Sinha, and Z. Zhou, Phys. Rev. Lett. **93**, 012701 (2004).
[6] C. L. Jiang, K. E. Rehm, H. Esbensen, R. V. F. Janssens, B. B. Back, C. N. Davids, J. P. Greene, D. J. Henderson, C. J. Lister, R. C. Pardo, T. Pennington, D. Peterson, D. Seweryniak, B. Shumard, S. Sinha, X. D. Tang, I. Tanihata, S. Zhu, P. Collon, S. Kurtz, and M. Paul, Phys. Rev. C **71**, 044613 (2005).
[7] A. M. Stefanini, G. Montagnoli, L. Corradi, S. Courtin, E. Fioretto, A. Goasduff, F. Haas, P. Mason, R. Silvestri, P. P. Singh, F. Scarlassara, and S. Szilner, Phys. Rev. C **82**, 014614 (2010).
[8] C. L. Jiang, A. M. Stefanini, H. Esbensen, K. E. Rehm, L. Corradi, E. Fioretto, P. Mason, G. Montagnoli, F. Scarlassara, R. Silvestri, P. P. Singh, S. Szilner, X. D. Tang, and C. A. Ur, Phys. Rev. C **82**, 041601(R) (2010).
[9] G. Montagnoli, A. M. Stefanini, C. L. Jiang, H. Esbensen, L. Corradi, S. Courtin, E. Fioretto, A. Goasduff, F. Haas, A. F. Kifle, C. Michelagnoli, D. Montanari, T. Mijatović, K. E. Rehm, R. Silvestri, P. P. Singh, F. Scarlassara, S. Szilner, X. D. Tang, and C. A. Ur, Phys. Rev. C **85**, 024607 (2012).
[10] G. Montagnoli, A. M. Stefanini, L. Corradi, S. Courtin, E. Fioretto, F. Haas, D. Lebhertz, F. Scarlassara, R. Silvestri, and S. Szilner, Phys. Rev. C **82**, 064609 (2010).
[11] G. Montagnoli, A. M. Stefanini, H. Esbensen, C. L. Jiang, L. Corradi, S. Courtin, E. Fioretto, A. Goasduff, J. Grebosz, F. Haas, M. Mazzocco, C. Michelagnoli, T. Mijatovic, D. Montanari, C. Parascandolo, K. E. Rehm, F. Scarlassara, S. Szilner, X. D. Tang, and C. A. Ur, Phys. Rev. C **87**, 014611 (2013).
[12] C. L. Jiang, A. M. Stefanini, H. Esbensen, K. E. Rehm, S. Almaraz-Calderon, B. B. Back, L. Corradi, E. Fioretto, G. Montagnoli, F. Scarlassara, D. Montanari, S. Courtin, D. Bourgin, F. Haas, A. Goasduff, S. Szilner, and T. Mijatovic, Phys. Rev. Lett. **113**, 022701 (2014).
[13] C. L. Jiang, B. B. Back, H. Esbensen, J. P. Greene, R. V. F. Janssens, D. J. Henderson, H. Y. Lee, C. L. Lister, M. Notani, R. C. Pardo, N. Patel, K. E. Rehm, D. Seweryniak, B. Shumard, X. Wang, S. Zhu, S. Mişicu, P. Collon, and X. D. Tang, Phys. Rev. C **78**, 017601 (2008).
[14] M. Dasgupta, D. J. Hinde, A. Diaz-Torres, B. Bouriquet, C. I. Low, G. J. Milburn, and J. O. Newton, Phys. Rev. Lett. **99**, 192701 (2007).
[15] A. M. Stefanini, G. Montagnoli, H. Esbensen, L. Corradi, S. Courtin, E. Fioretto, A. Goasduff, J. Grebosz, F. Haas, M. Mazzocco, C. Michelagnoli *et al.*, Phys. Lett. B **728**, 639 (2014).
[16] A. Shrivastava, K. Mahata, S. K. Pandit, V. Nanal, T. Ichikawa, K. Hagino, A. Navin, C. S. Palshetkar, V. V. Parkar, K. Ramachandran, P. C. Rout, A. Kumar, A. Chatterjee, and S. Kailas, Phys. Lett. B **755**, 332 (2016).
[17] A. Shrivastava, A. Navin, A. Lemasson, K. Ramachandran, V. Nanal, M. Rejmund, K. Hagino, T. Ichikawa, S. Bhattacharyya, A. Chatterjee, S. Kailas, K. Mahata, V. V. Parkar, R. G. Pillay, and P. C. Rout, Phys. Rev. Lett. **103**, 232702 (2009).
[18] A. Shrivastava, K. Mahata, V. Nanal, S. K. Pandit, V. V. Parkar, P. C. Rout, N. Dokania, K. Ramachandran, A. Kumar, A. Chatterjee, and S. Kailas, Phys. Rev. C **96**, 034620 (2017).
[19] G. Montagnoli, A. M. Stefanini, C. L. Jiang, K. Hagino, F. Galtarossa, G. Colucci, S. Bottoni, C. Broggini, A. Caciolli, P. Colovic, L. Corradi, S. Courtin, R. Depalo, E. Fioretto, G. Fruet, A. Gal, A. Goasduff, M. Heine, S. P. Hu, M. Kaur, T. Mijatovic, M. Mazzocco, D. Montanari, F. Scarlassara, E. Strano, S. Szilner, and G. X. Zhang, Phys. Rev. C **97**, 024610 (2018).
[20] A. Pakou, L. Acosta, P. D. O'Malley, S. Aguilar, E. F. Aguilera, M. Baines, D. Bardayan, F. D. Becchetti, C. Boomershine, M. Brodeur, F. Cappuzzello, S. Carmichael, L. Caves, E. Chávez, C. Flores-Vázquez, A. Gula, J. J. Kolata, B. Liu, D. J. Marín-Lámbarri, F. F. Morales, K. Rusek, A. M. Sánchez-Benítez, O. Sgouros, V. R. Sharma, V. Soukeras, and G. Souliotis, Phys. Rev. C **102**, 031601(R) (2020).
[21] S. Mişicu and H. Esbensen, Phys. Rev. Lett. **96**, 112701 (2006).
[22] S. Mişicu and H. Esbensen, Phys. Rev. C **75**, 034606 (2007).
[23] T. Ichikawa, K. Hagino, and A. Iwamoto, Phys. Rev. Lett. **103**, 202701 (2009).
[24] T. Ichikawa, Phys. Rev. C **92**, 064604 (2015).
[25] C. Simenel, A. S. Umar, K. Godbey, M. Dasgupta, and D. J. Hinde, Phys. Rev. C **95**, 031601(R) (2017).

[26] P. Möller, A. J. Sierk, T. Ichikawa, and H. Sagawa, At. Data Nucl. Data Tables **109–110**, 1 (2016).
[27] K. Kumar, T. Ahmad, S. Ali, I. A. Rizvi, A. Agarwal, R. Kumar, K. S. Golda, and A. K. Chaubey, Phys. Rev. C **87**, 054328 (2013).
[28] J. F. Ziegler, M. D. Ziegler, and J. P. Biersack, Nucl. Instrum. Methods B **268**, 1818 (2010).
[29] R. Brun and F. Rademakers, Nucl. Instrum. Methods Phys. Res. A **389**, 81 (1997).
[30] https://www.nndc.bnl.gov.
[31] P. R. S. Gomes and T. J. P. Penna, Nucl. Instrum. Methods Phys. Res. A **280**, 395 (1989).
[32] M. Cavinato, E. Fabrici, E. Gadioli, E. Gadioli Erba, P. Vergani, M. Crippa, G. Colombo, I. Redaelli, and M. Ripamonti, Phys. Rev C **52**, 2577 (1995).
[33] A. Gavron, Phys. Rev. C **21**, 230 (1980).
[34] R. L. Walter and P. P. Guss, Radiation Effects **95**, 73 (1986).
[35] L. McFadden and G. R. Satchler, Nucl. Phys. **84**, 177 (1966).
[36] C. L. Jiang, B. B. Back, H. Esbensen, R. V. F. Janssens, and K. E. Rehm, Phys. Rev. C **73**, 014613 (2006).
[37] C. L. Jiang, B. B. Back, R. V. F. Janssens, and K. E. Rehm, Phys. Rev. C **75**, 057604 (2007).
[38] E. S. Zin Thein, N. W. Lwin, and K. Hagino, Phys. Rev. C **85**, 057602 (2012).
[39] C. L. Jiang, K. E. Rehm, B. B. Back, and R. V. F. Janssens, Phys. Rev. C **79**, 044601 (2009).
[40] K. Hagino, N. Rowley, and A. T. Kruppa, Comput. Phys. Commun. **123**, 143 (1999).
[41] C. Y. Wong, Phys. Rev. Lett. **31**, 766 (1973).
[42] K. Hagino and S. Sakaguchi, Phys. Rev. C **100**, 064614 (2019).
[43] A. Mukherjee, Subinit Roy, M. K. Pradhan, M. Saha Sarkar, P. Basu, B. Dasmahapatra, T. Bhattacharya, S. Bhattacharya, S. K. Basu, A. Chatterjee, V. Tripathi, and S. Kailas, Phys. Lett. B **636**, 91 (2006).
[44] S. Raman, C. H. Malarkey, W. T. Milner, C. W. Nestor Jr., and, P. H. Stelson, At. Data Nucl. Data Tables **36**, 1 (1987).
[45] C. L. Jiang, B. B. Back, H. Esbensen, R. V. F. Janssens, Ş. Mişicu, K. E. Rehm, P. Collon, C. N. Davids, J. Greene, D. J. Henderson *et al.*, Phys. Lett. B **640**, 18 (2006).
[46] C. L. Jiang, K. E. Rehm, H. Esbensen, B. B. Back, R. V. F. Janssens, P. Collon, C. M. Deibel, B. DiGiovine, J. M. Figueira, J. P. Greene, D. J. Henderson, H. Y. Lee, M. Notani, S. T. Marley, R. C. Pardo, N. Patel, D. Seweryniak, X. D. Tang, C. Ugalde, and S. Zhu, Phys. Rev. C **81**, 024611 (2010).
[47] A. Mukherjee, M. Dasgupta, D. J. Hinde, K. Hagino, J. R. Leigh, J. C. Mein, C. R. Morton, J. O. Newton, and H. Timmers, Phys. Rev. C **66**, 034607 (2002).
[48] A. M. Stefanini, G. Montagnoli, R. Silvestri, L. Corradi, S. Courtin, E. Fioretto, B. Guiot, F. Haas, D. Lebhertz, P. Mason, F. Scarlassara, and S. Szilner, Phys. Lett. B **679**, 95 (2009).
[49] A. Navin, A. Chatterjee, S. Kailas, A. Shrivastava, P. Singh, and S. S. Kapoor, Phys. Rev. C **54**, 767 (1996).
[50] V. Tripathi, A. Navin, K. Mahata, K. Ramachandran, A. Chatterjee, and S. Kailas, Phys. Rev. Lett. **88**, 172701 (2002).
[51] O. Akyüz and A. Winther, in *Proceedings of the International School of Physics "Enrico Fermi,"* edited by R. A. Broglia, R. A. Ricci, and C. H. Dasso (North-Holland, Amsterdam, 1981), p. 492.